OPEN

Spinal Cord Astroblastoma With *EWSR1-BEND2* Fusion in Female Patients

A Report of Four Cases From China and a Comprehensive Literature Review

Lingyi Fu, PhD,† I. Weng Lao, MD,‡§‖ Liyun Huang, PhD,*† Liqiong Ou, PhD,¶ Lei Yuan, MD,*† Ziteng Li, MD,*† Shuo Li, PhD,*† Wanming Hu, MD,*† and Shaoyan Xi, MD*†*

Abstract: Astroblastoma is an extremely rare central nervous system tumor characterized by astroblastic pseudorosettes and vascular hyalinization. Despite these histologic hallmarks, its morphology can vary, occasionally resembling other central nervous system tumors such as ependymoma. A novel tumor entity, astroblastoma, meningioma 1 (*MN1*)-altered, has been identified, featuring *MN1* gene rearrangements typically involving BEN-domain containing 2 (*BEND2*) as a fusion partner. Most astroblastomas arise in the cerebral hemisphere. Here, we report 4 cases of spinal cord astroblastoma in female patients, all showing Ewing sarcoma RNA-binding protein 1 fusion with *BEND2*, rather than *MN1*. These tumors displayed growth patterns akin to traditional intracranial astroblastomas, with three cases demonstrating high-grade histology, including elevated mitotic activity and necrosis. Interestingly, some cases exhibited positive staining for pan-cytokeratin and hormone receptors. DNA methylation profiling clustered three of the four cases with the reference "AB_EWSR," whereas one case exhibited an independent methylation signature near the reference methylation group "AB_EWSR" and "pleomorphic xanthoastrocytoma." Together with the existing literature, we summarized a total of eleven cases, which predominantly affected children and young adults with female predilection. Eight of 10 patients experienced recurrence, underscoring the aggressive nature of this disease. We suggest recognizing a new molecular subgroup of spinal astroblastoma and recommend testing newly diagnosed infratentorial astroblastomas for Ewing sarcoma RNA-binding protein 1-BEND2 fusion.

Key Words: astroblastoma, spinal cord, EWSR1, BEND2

(*Am J Surg Pathol* 2024;48:1372–1380)

From the *State Key Laboratory of Oncology in South China, Guangdong Provincial Clinical Research Center for Cancer; †Department of Pathology, Sun Yat-sen University Cancer Center, Guangzhou; ‡Department of Pathology, Fudan University Shanghai Cancer Center; §Department of Oncology, Shanghai Medical College; ‖Institute of Pathology, Fudan University, Shanghai; and ¶Department of Pathology, Jiangmen Central Hospital, Jiangmen, China.

L.F., I.W.L., and L.H. contributed equally to this work.

This study was supported by grants from the National Natural Science Foundation of China (82203530 and 82102877), Guangdong Fundamental and Applied Fundamental Research Fund (2021A1515110959 and 2023A1515010158), and Guangzhou Municipal Science and Technology Project (202201011328).

Conflicts of Interest and Source of Funding: The authors have disclosed that they have no significant relationships with, or financial interest in, any commercial companies pertaining to this article.

Correspondence: Shaoyan Xi, MD, Department of Pathology, Sun Yat-sen University Cancer Center, 651 Dongfeng Road East, Guangzhou 510000, China (e-mail: xishy@sysucc.org.cn); Wanming Hu, MD, Department of Pathology, Sun Yat-sen University Cancer Center, 651 Dongfeng Road East, Guangzhou 510000, China (e-mail: huwm@sysucc.org.cn).

DOI: 10.1097/PAS.0000000000002298

Astroblastoma, *MN1*-altered was recently incorporated into the fifth edition of the World Health Organization (WHO) classification of CNS tumors as a new entity among the category of "circumscribed astrocytic gliomas."[1] The tumorigenesis of this disease is primarily driven by acquired fusions of the *MN1* gene, most commonly with the *BEND2* gene (*MN1*:*BEND2*), and less frequently with the CXXC-type zinc finger protein 5 (*CXXC5*) gene (*MN1*:*CXXC5*).[2] Typically located in the cerebral hemisphere, astroblastoma shows a significant female predilection, affecting patients 2 months to 40 years of age. Spinal astroblastoma is exceedingly rare, with only isolated cases documented in the literature.[3–6] Data regarding outcomes for astroblastoma patients are scarce, and no clear association has been established between specific clinical, histological, or molecular features and prognosis.[7]

The diagnosis of astroblastoma presents challenges due to histological and radiographic similarities with other CNS tumors, such as ependymoma, astrocytoma, and primitive neuroectodermal tumors. The lack of a definitive immunohistochemical profile further complicates the diagnosis.[8] Microscopically, astroblastoma is charac-

terized by astroblastic pseudorosettes and often exhibits prominent perivascular hyalinization.[9] Tumor cells typically show strong immunoreactivity for glial fibrillary acidic protein (GFAP), oligodendrocyte transcription factor 2 (Olig2), and S-100, with variable cytoplasmic or membranous epithelial membrane antigen (EMA) staining. Conversely, they are negative for isocitrate dehydrogenase 1 R132H. It has been noted that although histologically defined astroblastomas are molecularly diverse, those with *MN1* rearrangement tend to have a more favorable prognosis.[10] However, not all tumors displaying the morphology of astroblastoma exhibit *MN1* gene alteration. Novel fusions, such as *MAMLD1:BEND2*, *YAP1:BEND2,* and *EWSR1:EZHIP*, were reported.[6,11–13] *BRAF V600E* mutation was also presented.[14]

In this report, we analyzed 4 cases of female patients with astroblastoma, focusing on their uncommon spinal cord location and the unique molecular feature of *EWSR1-BEND2* fusion. All cases underwent next-generation sequencing (NGS), RNA sequencing (RNA-seq), fluorescence in situ hybridization (FISH), and DNA methylation profiling. We propose the establishment of a new tumor entity, spinal astroblastoma with *EWSR1-BEND2* fusion, as a major molecular subgroup of astroblastoma, predominantly affecting female individuals and associated with an aggressive clinical course.

MATERIALS AND METHODS

Collection of Tumor Specimens and Clinical Data

In this retrospective study, 4 cases of histologically diagnosed astroblastoma were analyzed from multiple collaborating centers for a 5-year period (2019 to 2024). Genotype checking was performed for all cases to ensure exclusion of material duplication from the same patient across centers. The histology of these cases was reviewed, and an extended immunohistochemistry (IHC) panel was conducted to support the diagnosis. Clinical features, demographics, radiological imaging findings, and follow-up details, where available, were extracted from the case records. Progression-free survival (PFS) was defined as the duration from diagnosis to tumor recurrence or death, whereas overall survival (OS) was defined as the duration from diagnosis to death from any cause.

Written consent was obtained from all patients or their legal representatives. All patients were anonymous. Ethical approval was granted by the Sun Yat-sen University Cancer Center Institute Research Ethics Committee, and all procedures adhered to the International Ethical Guidelines for Biomedical Research Involving Human Subjects.

Histological and IHC Analysis

All cases were processed as formalin-fixed and paraffin-embedded (FFPE) specimens, with sections cut to 4- to 5-μm thickness and stained using hematoxylin and eosin. Histological assessment included examination for cellularity, pseudorosette formation, microvascular proliferation, necrosis, and mitotic activity.

For IHC, samples were incubated in a 60°C oven for 2 hours, then deparaffinized in dimethylbenzene twice for 10 minutes, followed by rehydration in a graded ethanol series (100%, 95%, 90%, 80%, and 70%), and washed with distilled water. Antigen retrieval was achieved by subjecting slides to high-pressure pretreatment in citrate buffer (pH 6.0) for 2 minutes and blocking endogenous peroxidase activity with 0.3% H_2O_2 at 25°C for 30 minutes. Slides were then incubated in a blocking solution containing 5% horse serum, 3% BSA, and 0.1% Tween-20 in PBS for 1 hour at 25°C, followed by overnight incubation with primary antibodies at 4°C in a humidified chamber. The following day, slides were incubated with horseradish peroxidase -labeled goat antirabbit IgG for 1 hour at 25°C, washed with PBS, stained with 3,30-diaminobenzidine tetrahydrochloride, and counterstained with hematoxylin.

Primary antibodies used included GFAP (clone UMAB129, ZM-0118, and ZSGB-BIO), Olig2 (clone EP112, ZA-0561, and ZSGB-BIO), isocitrate dehydrogenase 1 R132H (clone OTI3G9, ZM-0447, and ZSGB-BIO), alpha-thalassemia/mental retardation syndrome X-linked protein (ZA-0016 and ZSGB-BIO), S-100 (clone 15E2E2 +4C4.9, ZM-0224, and ZSGB-BIO), EMA (clone GP1.4, ZM-0095, and ZSGB-BIO), pan-cytokeratin (CK) (clone AE1/AE3, ZM-0069, and ZSGB-BIO), p53 (clone DO-7, ZM-0408, and ZSGB-BIO), H3K27M (clone RM192, ZA-0321, and ZSGB-BIO), H3K27Me3 (clone RM175, ZA-0327, and ZSGB-BIO), and Ki67 (clone MIB-1, ZM-0167, and ZSGB-BIO).

Molecular Analysis

Targeted NGS was performed on all cases using a brain tumor-targeted gene panel, which included matched normal and tumor pairs. The panel, consisting of 353 genes closely related to CNS tumors, was validated by the Department of Pathology of Sun Yat-sen University. Genomic DNA and RNA were extracted from FFPE tumor samples using the Maxwell RSC DNA/RNA FFPE Kit (Promega) following the manufacturer's instructions. The high-throughput assay was performed using the NextSeq 550Dx as per the manufacturer's protocol. This involved submitting adapter-ligated and indexed cDNA or sheared genomic DNA to 2 hybridization and target-capture steps, followed by library amplification by polymerase chain reaction (PCR), cleaning, quantification, normalization, and pooling. Sequencing was performed on the Illumina NextSeq platform, using 101 cycles paired-end sequencing. Subsequently, the sequencing data were processed and analyzed using an in-house custom bioinformatics pipeline.

Telomerase reverse transcriptase (*TERT*) promoter mutations were evaluated using droplet digital PCR. Droplets were created using the AutoDG Droplet Digital PCR System QX200, and quantitative PCR was conducted on the QX200 Droplet Digital PCR System. For TERT promoter mutation determination, the dHsaEXD72405942 and dHsaEXD46675715 TaqMan probes (Biorad) were used according to the manufacturer's

instructions.

Methylguanine methyltransferase (*MGMT*) promoter methylation was assessed using pyrosequencing, which was performed using the PyroMark Q96 MGMT kit (Qiagen) according to the manufacturer's instructions.

Fluorescence In Situ Hybridization

FISH analysis was performed to detect the break-apart of *EWSR1*. FFPE sections were deparaffinized in xylene for 10 minutes, followed by washing in 100% ethanol, air-drying, and incubation in 2× sodium saline citrate (SSC) at 72°C for 40 minutes. Subsequently, sections were incubated in a proteinase K solution (500 mg/mL in 2× SSC) at 45°C for 5 to 80 minutes, washed in 2× SSC for 3 minutes at room temperature, and stored in 70% ethanol at 48°C. FISH was conducted using the SureFISH *EWSR1* probe (Agilent), which labels the human chromosomal *EWSR1* gene 5′ with a green signal (*EWSR1* 5′ BA 564 kb Green, Human Chr22: 29100656–29664246) and the *EWSR1* gene 3′ with a red signal (*EWSR1* 3′ BA 263 kb, red, Human Chr22: 29695821-29958416). All FISH procedures were performed according to the manufacturer's protocol, visualizing a minimum of 100 nuclei per slide. A positive score was assigned when at least 10% of the nuclei exhibited a break-apart signal. Each series of experiments included examination of a positive control slide from an Ewing sarcoma case known to harbor *EWSR1* rearrangement.

DNA Methylation-based Clustering

DNA was extracted from FFPE tissues using the Maxwell RSC DNA FFPE Kit (Promega) following the manufacturer's instructions. DNA concentration was determined using the Qubit dsDNA BR Assay kit (Invitrogen) per the manufacturer's protocol. Genome-wide DNA methylation profiling was performed following the Illumina Infinium Human Methylation protocol. The 850K methylation chip was used to assess the methylation status of 850,000 CpG sites in the human genome, covering promoters, coding regions, CpG islands, and enhancers found in the encyclopedia of DNA elements (ENCODE) and functional annotation of the mammalian genome (FANTOM) projects. The methylation data were analyzed using the Heidelberg methylation brain tumor classifier algorithm (http://www.molecularneuropathology.org) to establish methylation classes (MCs) correlating with brain tumor entities in the WHO classification.[15] Classifier scores with a probability above 0.9 were taken as indicative for the respective MCs.

Literature Review

A thorough literature search was performed on PubMed (http://www.ncbi.nlm.nih.gov/pubmed/) to identify previously reported cases of astroblastoma. Different combinations of keywords, including "astroblastoma," "MN1," "BEND2," "high-grade neuroepithelial tumor," and "EWSR1," were utilized in the title/abstract field. Redundant cases from multiple articles were combined for analysis.

Statistical Analysis

The $\chi 2$ test was used to compare categorical variables, and survival analysis was performed using the Kaplan-Meier method, with comparison made using the log-rank test. Survival time was measured in months from diagnosis. Statistical analysis was carried out using SPSS 26.0 software, and significance was set at *a* P value of < 0.05.

RESULTS

Clinical Case Summaries

Case 1

An 8-year-old girl presented with weakness in her left lower limb and claudication, along with complaints of difficulty in defecation, but no fever, headache, nausea, or vomiting. MRI revealed an intramedullary tumor located at the 8 to 9 thoracic vertebrae. Surgical resection successfully achieved total tumor removal. After surgery, she did not undergo additional treatment and remained asymptomatic. However, recurrence of the tumor at the same site was detected on MRI during the 12-month follow-up. The patient is currently hospitalized and preparing for the second surgery.

Case 2

A 14-year-old girl presented with progressively worsening neck pain over 6 months and limb weakness for 1 week in March 2018. MRI revealed an intramedullary mass at the C6-T1 level, which was pathologically diagnosed as a "high-grade neuroepithelial tumor" postoperatively. After surgery, she received radiotherapy at a local hospital and remained symptom-free for 5 years. However, in November 2023, she experienced a recurrence of limb weakness without numbness or pain. MRI confirmed tumor recurrence at the C6-C7 level, displaying solid and cystic components. She underwent surgical resection of the tumor at our hospital and is currently undergoing concurrent chemoradiotherapy. A follow-up MRI at 3 months postsurgery showed no signs of recurrence.

Case 3

A 35-year-old woman presented with lumbago and left leg pain persisting for 1.5 months. MRI revealed an intramedullary mass at the L1 level, which was pathologically diagnosed as a "high-grade neuroepithelial tumor" postoperatively. Following surgery, the patient did not receive additional treatment. However, at the 5-month follow-up, MRI showed tumor recurrence at the same location, prompting initiation of chemotherapy with temozolomide (TMZ). A second surgical resection was performed 9 months after the initial operation, followed by concurrent chemoradiotherapy. Subsequent MRI at 1-month postsurgery revealed no signs of recurrence.

Case 4

A 45-year-old woman presented with leg numbness and progressive difficulty in walking for a period of 2 years. MRI revealed an intramedullary tumor spanning

the 6 to 9 thoracic vertebrae. Subtotal resection was performed due to the unclear boundary between the tumor and the spinal cord. After surgery, the patient did not receive further treatment. At the 4-month postoperative follow-up, she experienced an uneventful recovery without neurological deficits, with MRI showing stable tumor remnant.

Histopathological Characteristics

Microscopically, all 4 cases exhibited astroblastic pseudorosettes with papillary or pseudopapillary configurations radiating toward central blood vessels (Fig. 1A). In certain regions, these formations appeared as structured sheets interspersed with collagen-fibrillary matrix (Fig. 1B). Well-developed vasculature and prominent perivascular hyalinization were observed (Fig. 1C). Cases 1 to 3 were classified as high histological grade due to high cellularity and necrosis. They displayed relatively poorly differentiated cells with oval hyperchromatic nuclei and abundant eosinophilic cytoplasm (Fig. 1D). Focal tumoral necrosis was present, although high mitotic activity or microvascular proliferation was not evident (Fig. 1E). Case 2 exhibited a multifocal interface with adjacent brain parenchyma, suggestive of an invasive growth pattern (Fig. 1F). Case 4 was classified as low histological grade, characterized by monotonous oval or round cells with fine chromatin growing in a sheet-like or perivascular pattern in densely hyalinized stroma. No pleomorphic or bizarre tumor cells were identified.

Immunoreactivity of tumor cells varied for GFAP, with notable positivity in the perivascular papillary areas (Fig. 2A). Olig2 staining was predominantly negative or focally positive (Fig. 2B). EMA staining exhibited a membranous and cytoplasmic focal spot-like pattern (Fig. 2C). The expression of H3K27me3 was preserved. S-100 staining was positive (Fig. 2D). The Ki67 labeling index ranged from 1% to 30% (Figs. 2E, F). Tumor cells demonstrated strong and diffuse positive staining for CK (AE1/AE3) (Fig. 2G). Variable immunoreactivity for estrogen receptor (ER) or progesterone receptor (PR) was observed in some tumor cells (Figs. 2H, I).

Gene Expression Profiling

NGS revealed an *EWSR1* fusion with *BEND2* as the 3′ partner. In cases 1 and 2, the gene fusion involved exons 1 to 7 of *EWSR1* and exons 2 to 14 of *BEND2* (Fig. 3A). Conversely, in cases 3 and 4, exon 3 of *EWSR1* fused with exon 8 of *BEND2*. The *EWSR1-BEND2* fusion was the sole identified oncogenic alteration in all 4 cases. No mutations affecting *IDH*, alpha-thalassemia/mental retardation syndrome X-linked protein, *CDKN2A/2B*, *EGFR*, *BRAF*, *NF1*, *FGFR*, *NTRK*, *PDGFRA*, *MET*, *PIK3CA*, *PIK3R1*, *PTEN*, *TP53*, *CIC*, *FUBP1*, *MN1*, *ZFTA* (*c11orf95*), *RELA*, *YAP1*, *MYC*, *MYCN*, *MYB*, *MYBL1*, or histone H3 genes were detected. In addition, no *TERT* promoter mutations or *MGMT* promoter methylation were observed in any of the cases. The break-apart of *EWSR1* was further confirmed by FISH (Fig. 3B). Although the quantity of chromosomal copy number aberrations varied, none of the tumors exhibited whole-arm co-deletion of chromosomes 1p and 19q, focal amplifications, or homozygous deletions (Fig. 3C).

DNA Methylation Profiling

All the 4 cases underwent DNA methylation profiling. We performed *t-SNE* analysis by using our cohort together with published reference cases, encompassing nearly all CNS tumor types and subtypes.[5,15,16] We further refined *t-SNE* analysis for better visualization by narrowing representative MCs. As shown in Figure 3D, cases 1, 2, and 4 clustered with the reference "AB_EWSR," whereas case 3 exhibited an independent methylation signature near the reference methylation group "AB_EWSR" and " pleomorphic xanthoastrocytoma."

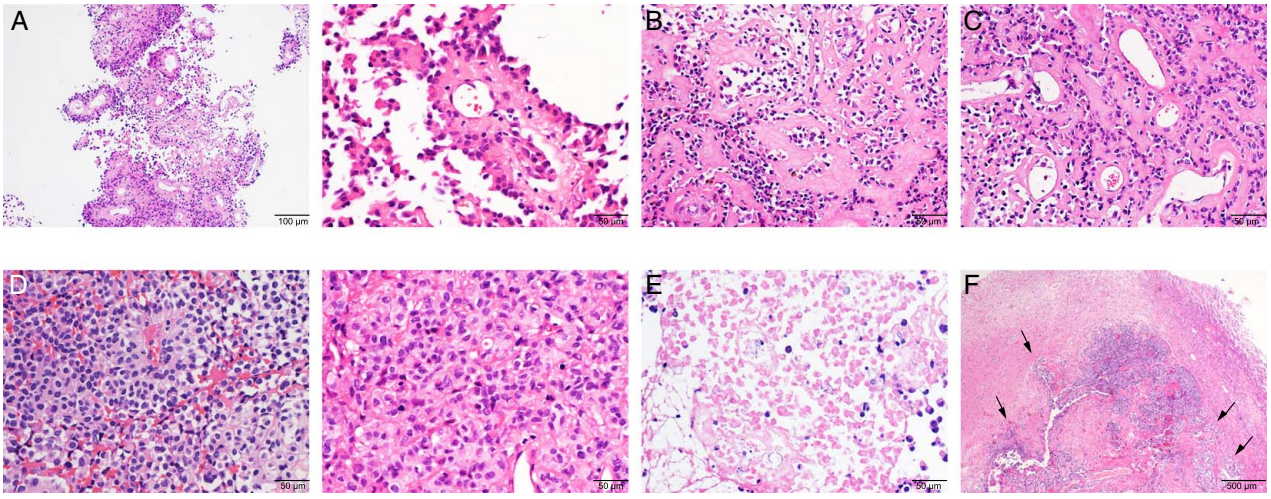

FIGURE 1. Histopathological features. A, Astroblastic pseudorosettes and papillary or pseudopapillary configurations around central blood vessels. B, Collagen-fibrillary stroma. C, Perivascular hyalinization. D, High cellularity. E, Tumoral necrosis. F, Multifocal interface with adjacent brain parenchyma.

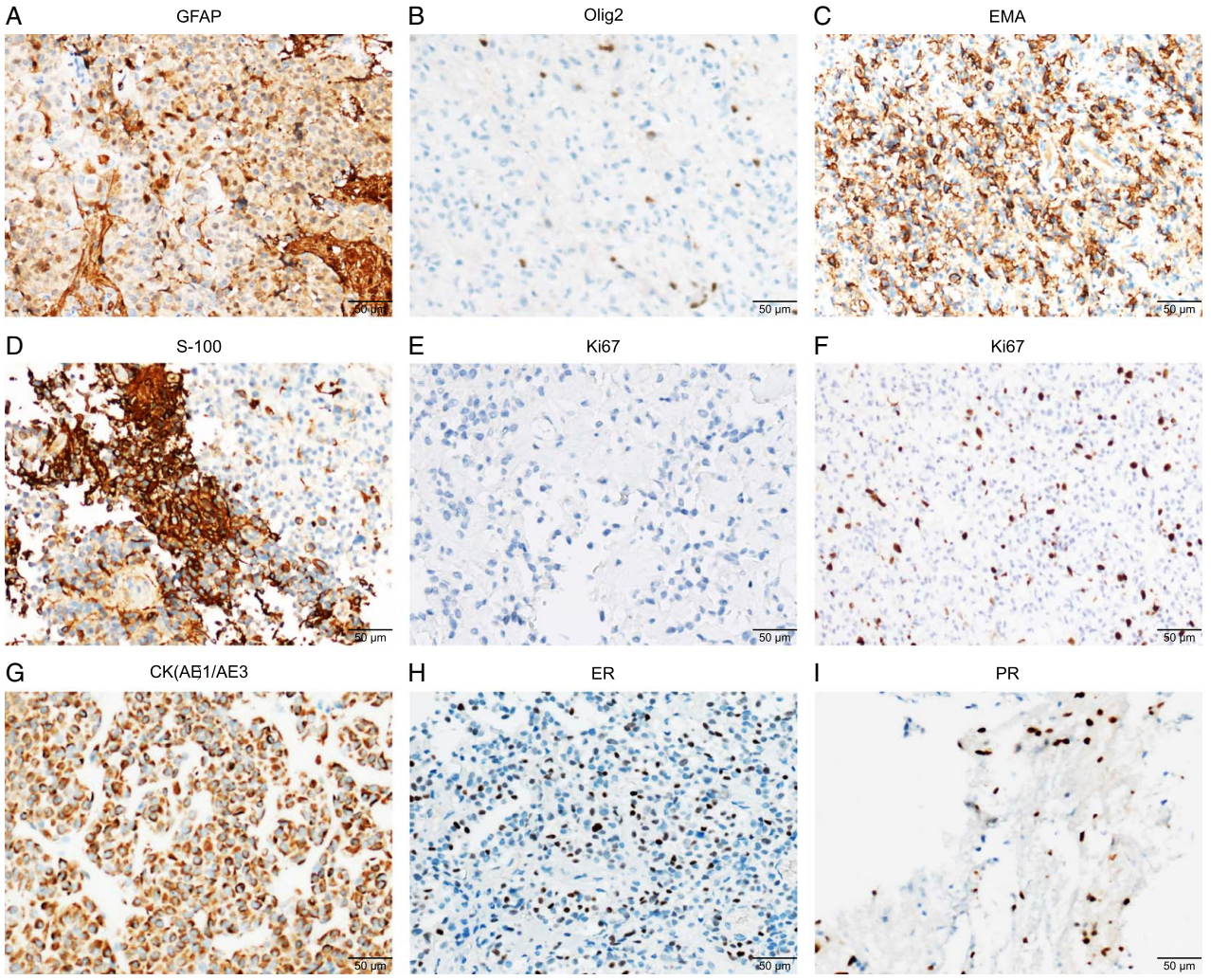

FIGURE 2. IHC staining. A, Variable GFAP staining, notably positive in the perivascular papillary areas. B, Focal Olig2 positive. C, Membranous and cytoplasmic focal spot-like staining for EMA. D, Positive S-100 staining. E, Representative image of low Ki67 labeling index. F, Representative image of high Ki67 labeling index. G, Positive staining for CK(AE1/AE3). H, Positive staining for ER. I, Positive staining for PR.

Using the online DKFZ Brain Tumor Classifier (www.molecularneuropathology.org), random forest classification confirmed a high-confidence match to the "astroblastoma, *MN1*-altered" methylation class in cases 1, 2, and 4.

Literature Review and Survival Analysis

Our study contributes to the existing literature, which now comprises eleven reported cases of astroblastomas harboring the *EWSR1-BEND2* fusion, with clinical follow-up data available for 10 cases[5,17–19] (Table 1). As illustrated in Figures 4A–C, this tumor predominantly affects children and young adults (7 of 11) with a median age of 20 years. Notably, there is a significant female predominance (7 of 11). The majority of patients experienced tumor recurrence (8 of 10) with a median PFS time of 20.88 months (Fig. 4D). More than half of the patients were alive at the time of the last follow-up (6 of 10). The median OS time after the initial surgery was 109.43 months (Fig. 4E).

DISCUSSION

The term "astroblastoma" was first coined by Bailey and Cushing in 1926 and further characterized by Bailey and Bucy in 1930.[20] Initially classified under "astrocytic tumors" in the first edition of the WHO classification of CNS tumors in 1979, it was later reclassified under "neuroepithelial tumors of uncertain histogenesis" and has remained there since the second edition in 1993.[21] The cell origin of astroblastoma has been debated. Rubinstein and Herman[22] suggested a possible cytogenic relationship to tanycytes, a glial cell type with features intermediate between astrocytes and ependymocytes. He categorized astroblastoma into low- or high-grade subtypes, although there have been discrepancies between histopathological

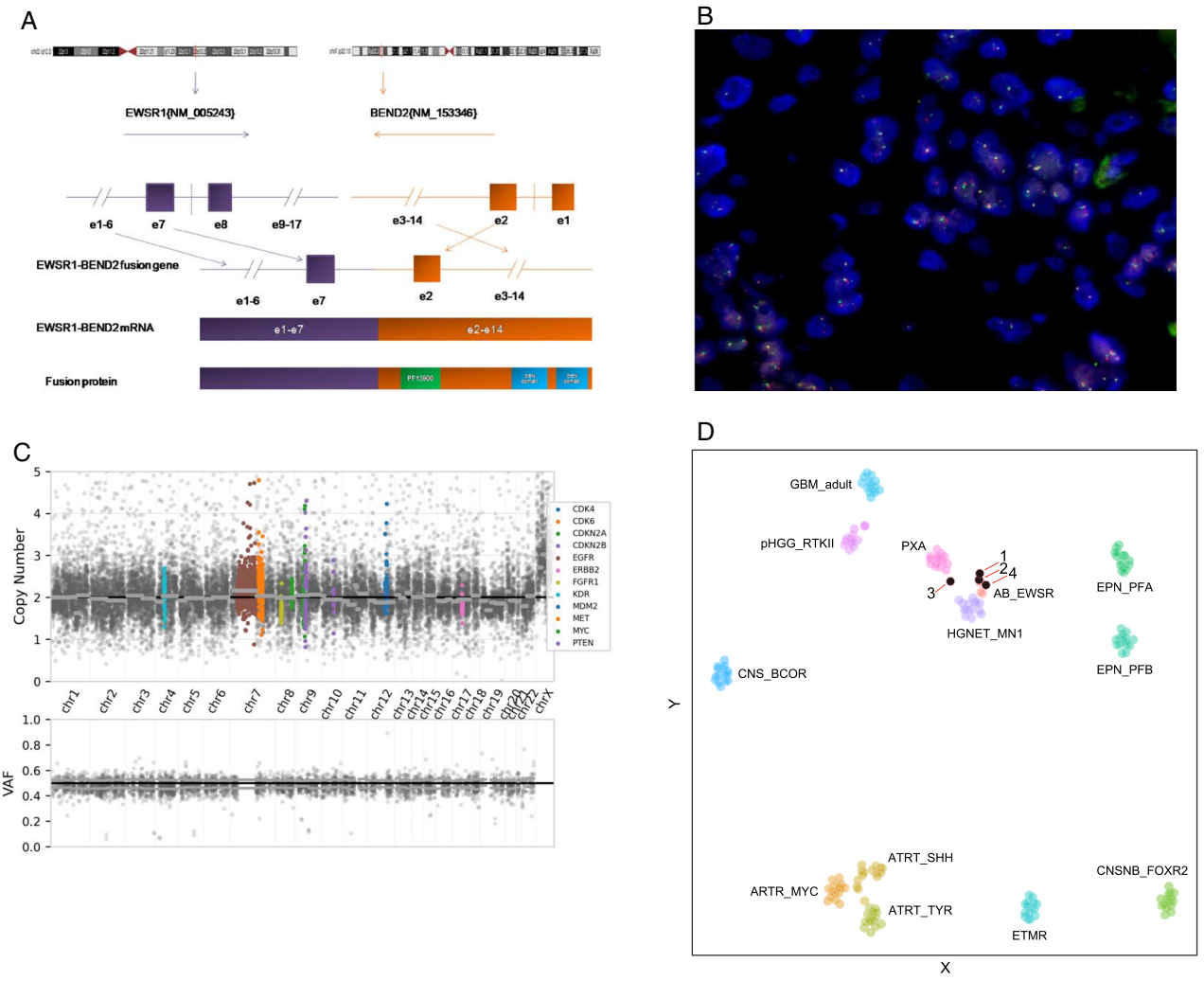

FIGURE 3. Gene expression and DNA methylation profiling. A, NGS revealed an in-frame *EWSR1-BEND2* fusion, with the breakpoint between *EWSR1* exon 3 and *BEND2* exon 8. B, FISH showing *EWSR1* fracture. C, Copy number variation profile. D, *t*-SNE clustering analysis.

features and prognosis.[23] To date, a definitive WHO grade has not been assigned to astroblastoma.

In 2016, Sturm et al[16] conducted a comprehensive molecular characterization of a large cohort of institutionally diagnosed CNS primitive neuroectodermal tumors and identified "high-grade neuroepithelial tumor with *MN1* alteration (HGNET-*MN1*)" as a new CNS tumor entity characterized by rearrangement of the *MN1* gene. Subsequent studies supported the association of *MN1* rearrangement with astroblastoma.[24] In 2020, the

TABLE 1. Known Cases of Astroblastoma With *EWSR1-BEND2* Fusion

Patient	Age	Sex	Location	Postoperative therapy	Follow-up	Status	Reference
1	3 mo	M	Spinal cord	None	1M	Died	13
2	38 y	M	Brainstem	Radiation and chemotherapy	12M	Alive	12
3	36 y	M	Spinal cord	Radiation and chemotherapy	12M	Died	14
4	20 y	M	Brainstem	Unknown	1M	Unknown	6
5	6 y	F	Spinal cord	None	25M	Died	6
6	26 y	F	Right frontal lobe	Radiation and chemotherapy	117M	Died	6
7	6 y	F	Left frontal lobe	None	90M	Alive	6
8	8 y	F	Spinal cord	None	12M	Alive	Current study
9	14 y	F	Spinal cord	Chemoradiotherapy	63M	Alive, on therapy	Current study
10	35 y	F	Spinal cord	Chemoradiotherapy	15M	Alive, on therapy	Current study
11	45 y	F	Spinal cord	None	4M	Alive	Current study

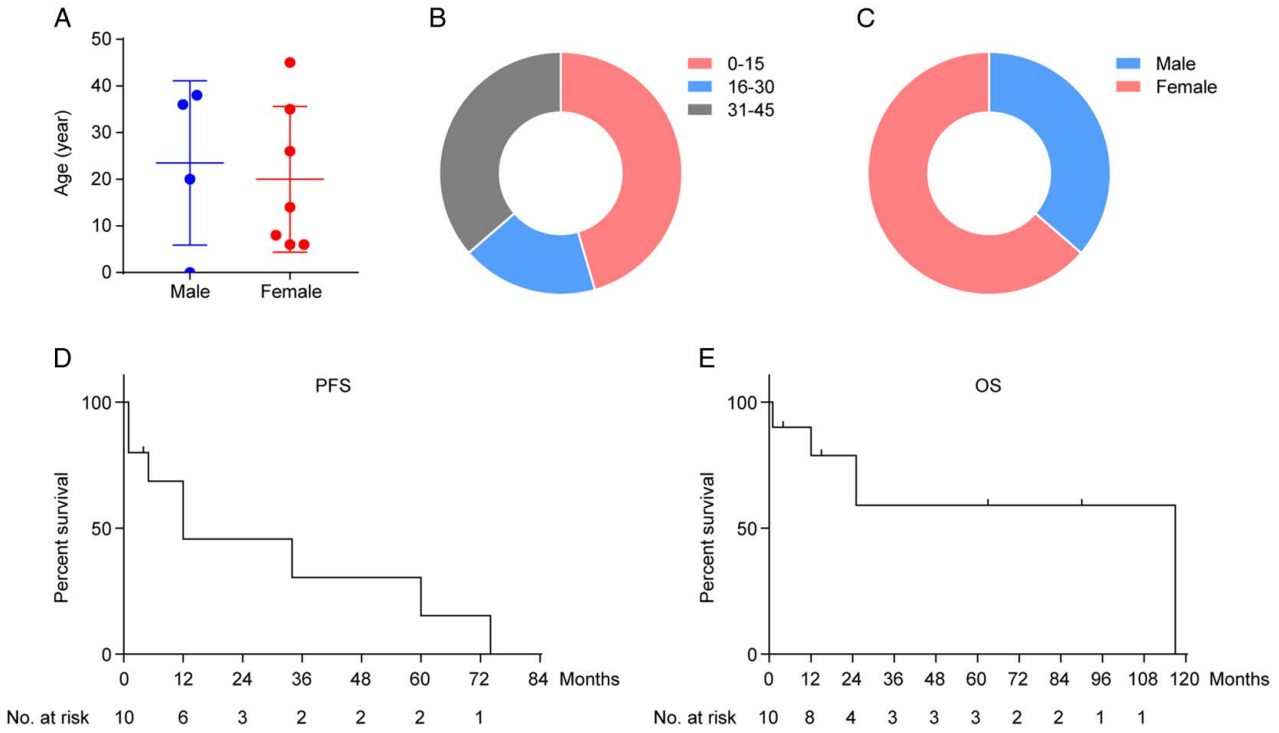

FIGURE 4. Survival analysis. A, Age and gender distribution of patients (n = 11). B, Age distribution of patients (n = 11, 0 to 30:31 to 45 = 7:4). C, Gender distribution of patients (n = 11, female: male = 7:4). D, Median PFS time of 20.88 months (n = 10). E. Median OS time of 109.43 months (n = 10).

Consortium to Inform Molecular and Practical Approaches to CNS Tumor Taxonomy (cIMPACT-NOW) recommended the term "astroblastoma, *MN1*-altered" for neoplasms with *MN1* alteration. Histologically, classic astroblastomas that lack *MN1* alterations and do not carry molecular alterations characteristic of other types of astrocytic or ependymal tumors, such as *BRAF V600E* mutation or *RELA* fusion, could be designated as "Astroblastoma, NEC".[25] The term "HGNET-*MN1*" was no longer recommended in the fifth edition of the WHO classification of CNS tumors.

Notably, not all tumors morphologically resembling astroblastomas exhibit *MN1* alteration. Astroblastoma, *MN1*-altered primarily occurs in the cerebral hemisphere. However, astroblastomas located in infratentorial regions such as the spinal cord or brainstem may more frequently exhibit uncommon fusions. Yamasaki et al[18] reported a case of a 3-month-old boy with an intramedullary spinal cord tumor harboring an *EWSR1-BEND2* fusion but no *MN1* fusion, who died of the disease 1 month after surgery. Smith-Cohn et al[17] reported a case of a 38-year-old man with a brainstem astroblastoma with *EWSR1-BEND2* fusion who underwent treatment with chemoradiation and TMZ, followed by adjuvant TMZ, without progression over 1 year. Tsutsui et al[19] reported a case of a 36-year-old man with a spinal cord astroblastoma showing *EWSR1-BEND2* fusion, who underwent concurrent chemoradiation therapy but was later found to have massive tumor dissemination 12 months later. Lucas et al[5] conducted the study with the largest sample size, performing targeted NGS and genome-wide DNA methylation profiling on a cohort of 4 patients with astroblastoma-like histologic features. These patients clustered into a single epigenetic subgroup most similar to the methylation class "astroblastoma" with all cases showing *EWSR1-BEND2* fusion. In addition, novel fusions such as *MAMLD1-BEND2* fusion in astroblastoma-like tumors in the spinal cord have also been reported.[6,11] Furthermore, *EWSR1-BEND2* fusion has been found not only in CNS tumors but also in low-grade sinonasal sarcoma,[26] salivary duct carcinoma,[27] and pancreatic neuroendocrine tumors.[28,29]

In this report, we describe 4 cases exhibiting morphological features of astroblastoma characterized by *EWSR1-BEND2* fusion. All 4 cases occurred in children and young adults and located in the spinal cord, with varying degrees of aggressiveness. Together with the existing literature, we summarized a total of 11 cases. This tumor predominantly affected female patients (7 of 11), which was consistent with supratentorial astroblastoma carrying *MN1-BEND2* fusion.[30]

Genome-wide DNA methylation assays were performed on all the cases, which clustered them into the "astroblastoma" subgroup. Morphologically, all 4 cases exhibited astroblastic pseudorosettes and collagen-fibrillary matrix. Three cases displayed high histological grade features such as high cellularity, pronounced necrosis, and hyperchromatic nuclei, whereas 1 case presented with fine chromatin without necrosis or mitotic activity. IHC

staining revealed focal or diffuse positivity for GFAP in all cases, with less positivity for Olig2. All cases were immunoreactive for EMA, with the expression pattern of EMA aiding in the differential diagnosis between astroblastoma and ependymoma. Interestingly, 3 cases showed positive staining for CK (AE1/AE3), which could lead to misdiagnosis with metastatic cancer or sarcoma. Positive hormone receptor staining, such as ER and PR, was observed in 2 cases, suggesting a potential role of hormones in this disease, in line with its female predominance. This shared similarities to meningioma which demonstrated a more than two-fold higher incidence among females with positive hormone receptor expression.[31,32]

The BEND family proteins interact with various proteins, primarily components of transcription-repressive complexes involved in chromatin remodeling or modification.[33–37] However, BEND2 remains poorly understood. Ma et al[38] reported that BEND2 inhibits genes involved in meiotic initiation, regulating chromatin accessibility and modifying H3K4me3 during mouse spermatogenesis. We propose that the consequences of *BEND2* fusion depend on the aberrant recruitment of the partner gene. *EWSR1* is vital in gene expression, meiotic and mitotic cell division, cell signaling, DNA repair, and cellular aging. *EWSR1* fusions are oncogenic in various benign and malignant tumors,[39,40] suggesting that the fusion of *EWSR1* and *BEND* genes may contribute to astroblastoma tumorigenesis.

MN1 alteration is associated with a favorable prognosis in intracranial astroblastomas. In one study, *MN1* rearrangements (n = 10) in 27 histologically defined astroblastomas correlated with better overall survival compared with other genetic subtypes.[10] Another study involving 40 gliomas indicated that upregulated *MN1* expression suggested extended OS and PFS.[41] A meta-analysis of *MN1*-altered neuroepithelial tumors (comprising 73 cases) showed 5- and 10-year progression-free survival rates of 38% and 0%, respectively, and 5- and 10-year OS rates of 89% and 55%, respectively.[2] In our study, 3 of 4 patients with spinal astroblastomas harboring *EWSR1-BEND2* fusion exhibited relatively high-grade morphology and an aggressive clinical course. Including literature cases, there are now 11 cases of astroblastomas with *EWSR1-BEND2* fusion, mostly in the spinal cord, with 8 of 10 patients experiencing tumor recurrence. *EWSR1-BEND2* fusion likely indicates poor survival and a high risk of recurrence, contrary to *MN1* outcomes.

EWSR1 is located at chromosome 22q12.2 near *MN1*, and both translocations involve the same 22q12 general breakpoint region.[42] Although the reasons for the higher prevalence of *EWSR1-BEND2* fusions in the spinal cord and brainstem compared with *MN1-BEND2* fusion in the hemisphere remain unclear, we propose that *BEND2* may play a more critical role in molecular oncogenesis and tumor classification of astroblastoma than *MN1*. The *EWSR1-BEND2* fusion likely initiates the tumorigenesis of spinal astroblastoma. Unfortunately, there is no reliable antibody to detect BEND2 at the protein level. This situation is reminiscent of supratentorial ependymoma, previously defined by *RELA* fusion according to the 2016 WHO classification of CNS tumors. The 2021 WHO classification now recognizes the newly defined ependymoma type *ZFTA* fusion-positive, which replaces the former definition and acknowledges *ZFTA* as an oncogenic driver fusion involving not only *RELA* but also other partners.[43]

In conclusion, we propose establishing tumors with *EWSR1-BEND2* fusion as a major molecular subgroup of infratentorial astroblastoma, characterized by high-grade histology (including necrosis and increased mitotic activity), indicating a poor prognosis. Further studies are necessary to fully define the biological and clinicopathological spectrum of astroblastomas, including establishing evidence-based grading criteria and determining optimal treatment regimens.

ACKNOWLEDGMENTS

The authors thank Jingping Yun, Jian Wang, Jun Hou, Qiuliang Wu, and Jing Zeng for their excellent technical assistance.

REFERENCES

1. Louis DN, Perry A, Wesseling P, et al. The 2021 WHO Classification of Tumors of the Central Nervous System: a summary. *Neuro Oncol*. 2021;23:1231–1251.
2. Chen W, Soon YY, Pratiseyo PD, et al. Central nervous system neuroepithelial tumors with MN1-alteration: an individual patient data meta-analysis of 73 cases. *Brain Tumor Pathol*. 2020;37:145–153.
3. Rao S, Nufina TA, Sugur H, et al. Spinal astroblastoma: a rare tumour in an unusual location. *Childs Nerv Syst*. 2022;38:1797–1801.
4. Yamada SM, Tomita Y, Shibui S, et al. Primary spinal cord astroblastoma: case report. *J Neurosurg Spine*. 2018;28:642–646.
5. Lucas CG, Gupta R, Wu J, et al. EWSR1-BEND2 fusion defines an epigenetically distinct subtype of astroblastoma. *Acta Neuropathol*. 2022;143:109–113.
6. Walker EN, Laws MT, Cozzi F, et al. A case of disseminated spinal astroblastoma harboring a MAMLD1::BEND2 fusion. *Neuropathology*. 2023;10:1111.
7. Horbinski C, Berger T, Packer RJ, et al. Clinical implications of the 2021 edition of the WHO classification of central nervous system tumours. *Nat Rev Neurol*. 2022;18:515–529.
8. Lehman NL. Central nervous system tumors with ependymal features: a broadened spectrum of primarily ependymal differentiation? *J Neuropathol Exp Neurol*. 2008;67:177–188.
9. Brat DJ, Hirose Y, Cohen KJ, et al. Astroblastoma: clinicopathologic features and chromosomal abnormalities defined by comparative genomic hybridization. *Brain Pathol*. 2000;10:342–352.
10. Lehman NL, Usubalieva A, Lin T, et al. Genomic analysis demonstrates that histologically-defined astroblastomas are molecularly heterogeneous and that tumors with MN1 rearrangement exhibit the most favorable prognosis. *Acta Neuropathol Commun*. 2019;7:42.
11. Rossi S, Barresi S, Colafati GS, et al. Paediatric astroblastoma-like neuroepithelial tumour of the spinal cord with a MAMLD1-BEND2 rearrangement. *Neuropathol Appl Neurobiol*. 2022;48:e12814.
12. Cuoco JA, Williams S, Klein BJ, et al. Astroblastoma With a Novel YAP1::BEND2 Fusion: A Case Report. *J Pediatr Hematol Oncol*. 2024;46:e313–e316.
13. Liu J, Sun D, Lin F, et al. An EWSR1-EZHIP fusion in a cerebral hemisphere astroblastoma. *Neuropathology*. 2023;43:340–344.
14. Lehman NL, Hattab EM, Mobley BC, et al. Morphological and molecular features of astroblastoma, including BRAFV600E mutations, suggest an ontological relationship to other cortical-based gliomas of children and young adults. *Neuro Oncol*. 2017;19:31–42.
15. Capper D, Jones DTW, Sill M, et al. DNA methylation-based classification of central nervous system tumours. *Nature*. 2018;555:469–474.

16. Sturm D, Orr BA, Toprak UH, et al. New Brain Tumor Entities Emerge from Molecular Classification of CNS-PNETs. *Cell*. 2016; 164:1060–1072.
17. Smith-Cohn MA, Abdullaev Z, Aldape KD, et al. Molecular clarification of brainstem astroblastoma with EWSR1-BEND2 fusion in a 38-year-old man. *Free Neuropathol*. 2021;2:2–16.
18. Yamasaki K, Nakano Y, Nobusawa S, et al. Spinal cord astroblastoma with an EWSR1-BEND2 fusion classified as a high-grade neuroepithelial tumour with MN1 alteration. *Neuropathol Appl Neurobiol*. 2020;46:190–193.
19. Tsutsui T, Arakawa Y, Makino Y, et al. Spinal cord astroblastoma with EWSR1-BEND2 fusion classified as HGNET-MN1 by methylation classification: a case report. *Brain Tumor Pathol*. 2021; 38:283–289.
20. Bailey P, Cushing H. *A classification of the tumors of the glioma group on a histogenetic basis with a correlated study of prognosis*. The J.B. Lippincott Co, Montreal. 1926.
21. Scheithauer BW. Development of the WHO classification of tumors of the central nervous system: a historical perspective. *Brain Pathol*. 2009;19:551–564.
22. Rubinstein LJ, Herman MM. The astroblastoma and its possible cytogenic relationship to the tanycyte. An electron microscopic, immunohistochemical, tissue- and organ-culture study. *Acta Neuropathol*. 1989;78:472–483.
23. Bonnin JM, Rubinstein LJ. Astroblastomas: a pathological study of 23 tumors, with a postoperative follow-up in 13 patients. *Neurosurgery*. 1989;25:6–13.
24. Hirose T, Nobusawa S, Sugiyama K, et al. Astroblastoma: a distinct tumor entity characterized by alterations of the X chromosome and MN1 rearrangement. *Brain Pathol*. 2018;28:684–694.
25. Louis DN, Wesseling P, Aldape K, et al. cIMPACT-NOW update 6: new entity and diagnostic principle recommendations of the cIMPACT-Utrecht meeting on future CNS tumor classification and grading. *Brain Pathol*. 2020;30:844–856.
26. Palsgrove DN, Manucha V, Park JY, et al. A Low-grade Sinonasal Sarcoma Harboring EWSR1::BEND2: Expanding the Differential Diagnosis of Sinonasal Spindle Cell Neoplasms. *Head Neck Pathol*. 2023;17:571–575.
27. Todorovic E, Dickson BC, Weinreb I. Salivary Gland Cancer in the Era of Routine Next-Generation Sequencing. *Head Neck Pathol*. 2020;14:311–320.
28. Scarpa A, Chang DK, Nones K, et al. Whole-genome landscape of pancreatic neuroendocrine tumours. *Nature*. 2017;543:65–71.
29. Agaimy A, Kasajima A, Stoehr R, et al. Gene fusions are frequent in ACTH-secreting neuroendocrine neoplasms of the pancreas, but not in their non-pancreatic counterparts. *Virchows Arch*. 2023;482: 507–516.
30. Lehman NL, Spassky N, Sak M, et al. Astroblastomas exhibit radial glia stem cell lineages and differential expression of imprinted and X-inactivation escape genes. *Nat Commun*. 2022;13:2083.
31. Miyagishima DF, Sundaresan V, Gutierrez AG, et al. A systematic review and individual participant data meta-analysis of gonadal steroid hormone receptors in meningioma. *J Neurosurg*. 2023;139: 1638–1647.
32. Wiemels J, Wrensch M, Claus EB. Epidemiology and etiology of meningioma. *J Neurooncol*. 2010;99:307–314.
33. Kaul-Ghanekar R, Jalota A, Pavithra L, et al. SMAR1 and Cux/CDP modulate chromatin and act as negative regulators of the TCRbeta enhancer (Ebeta). *Nucleic Acids Res*. 2004;32:4862–4875.
34. Bhattacharya A, Mukherjee S, Khan P, et al. SMAR1 repression by pluripotency factors and consequent chemoresistance in breast cancer stem-like cells is reversed by aspirin. *Sci Signal*. 2020;13: eaay6077.
35. Korutla L, Degnan R, Wang P, et al. NAC1, a cocaine-regulated POZ/BTB protein interacts with CoREST. *J Neurochem*. 2007;101: 611–618.
36. Kurniawan F, Prasanth SG. A BEN-domain protein and polycomb complex work coordinately to regulate transcription. *Transcription*. 2022;13:82–87.
37. Zhang J, Zhang Y, You Q, et al. Highly enriched BEND3 prevents the premature activation of bivalent genes during differentiation. *Science*. 2022;375:1053–1058.
38. Ma L, Xie D, Luo M, et al. Identification and characterization of BEND2 as a key regulator of meiosis during mouse spermatogenesis. *Sci Adv*. 2022;8:eabn1606.
39. Flucke U, van Noesel MM, Siozopoulou V, et al. EWSR1-The Most Common Rearranged Gene in Soft Tissue Lesions, Which Also Occurs in Different Bone Lesions: An Updated Review. *Diagnostics*. 2021;11:1093.
40. Thway K, Fisher C. Mesenchymal Tumors with EWSR1 Gene Rearrangements. *Surg Pathol Clin*. 2019;12:165–190.
41. Saini M, Jha AN, Tangri R, et al. MN1 overexpression with varying tumor grade is a promising predictor of survival of glioma patients. *Hum Mol Genet*. 2021;29:3532–3545.
42. Alhalabi KT, Stichel D, Sievers P, et al. PATZ1 fusions define a novel molecularly distinct neuroepithelial tumor entity with a broad histological spectrum. *Acta Neuropathol*. 2021;142:841–857.
43. Kresbach C, Neyazi S, Schuller U. Updates in the classification of ependymal neoplasms: The 2021 WHO Classification and beyond. *Brain Pathol*. 2022;32:e13068.